Proceedings of the ASME 2014 Dynamic Systems and Control Conference
DSCC2014
October 22-24, 2014, San Antonio, TX, USA

DSCC2014-5897

DYNAMIC MODEL AND SIMULATION OF FLAG VIBRATIONS MODELED AS A MEMBRANE

Gary Frey
Department of Mechanical Engineering
The University of Alabama
Tuscaloosa, AL 35487
gofrey@crimson.ua.edu

Ben Carmichael
Department of Mechanical Engineering
The University of Alabama
Tuscaloosa, AL 35487
bdcarmichael@crimson.ua.edu

Joshua Kavanaugh
Department of Mechanical Engineering
The University of Alabama
Tuscaloosa, AL 35487
kavan006@crimson.ua.edu

S. Nima Mahmoodi
Department of Mechanical Engineering
The University of Alabama
Tuscaloosa, AL 35487
nmahmoodi@eng.ua.edu

ABSTRACT

A flag is modeled as a membrane to investigate the two-dimensional characteristics of the vibration response to an uniform wind flow. Both the affecting tension and pressure functions for the wind flow with constant velocity are introduced and utilized in the modeling. In this case, the tension is caused by the weight of the flag. The pressure function is a function describing the pressure variations caused on the flag when in uniform flow. The pressure function is found by assuming that the air flow is relatively slow and that the flag is wide enough to minimize cross flow at the boundaries. An analysis of the downstream motion of the flag is necessary as well. Hamilton's principle is employed to derive the partial differential equation of motion. The flag is oriented in the vertical direction to neglect the effect of the flag's weight on the system's response. Galerkin's method is used to solve for the first four mode shapes of the system, and the system response is numerically solved. Simulations reveal a very reasonable model when the flag is modeled as a membrane.

NOMENCLATURE

α, β, γ Eigenvalues for the separated spatial functions

Δ Change in length of a line segment on the surface of the flag

δ Variational operator

ξ Velocity potential function of the fluid

$\hat{\xi}$ Separated two-dimensional spatial function of the potential function

ρ Area density of the membrane

ϕ Separated spatial function of x

ψ Separated spatial function of y

ω Eigenvalue for the separated time function

ω_{jk} Natural frequency of the jk^{th} mode

ω_{11} Natural frequency of the first mode

a Speed of sound in the fluid

A Area of the membrane

A_n, q_n Separation coefficients of the potential function

A, B, C, D, E Constant coefficient matrices of the time factors

c Wave speed in the membrane

G_{jk} Generalized set of coordinates representing the state-space transformation of the time factors

h Dimension of the flag in the x-direction

KE Kinetic energy

l_x Cosine function of the angle between the major axis of the flag

L Dimension of the flag in the y-direction

L Lagrangian of the system

q Separated function of time

Q_{jk} Time factor of the jk^{th} mode

t_1, t_2 Arbitrary, finite points in time

T Tension in the membrane

T_x Tension in the x-direction

T_y Tension in the y-direction

$\mathbf{v}$ Velocity vector field of the fluid

V Potential energy

V_{air} Scalar, freestream velocity of the fluid

w Deflection of the membrane

$\tilde{w}$ Assumed form of the deflection solution for the surface condition

$\hat{w}$ Experimental scaling coefficient

W_{jk} Mode shape of the jk^{th} mode

W^{nc} Non-conservative work

INTRODUCTION

Attempting to model a flag is not a new problem, for many researchers have taken various approaches. The motion of a flag has been studied by numerous people over the years. Generally, a flag is modeled as a beam, specifically an Euler-Bernoulli beam, in uniform flow [1-3]. For this to be done, the bending rigidity of the flag is assumed to be low. While modeling a flag this way has yielded favorable results, this paper will attempt to model the flag as a membrane. In modeling the flag as a membrane, the bending rigidity, or stiffness, of the flag is assumed to be negligible. Furthermore, the flag is assumed to be inextensible [4-5]. Modeling the system as a membrane should more accurately capture the dynamics of the system compared to modeling it as a beam.

Also, the flag is assumed to be in a clamped-free position. In other words, the leading edge is clamped, while the trailing edge is free. Thus, while one edge is clamped, the other three edges can freely deflect. This is a readily agreed upon configuration among those who have modeled flags. For the sake of this paper, the flag will be hanging vertically, and the fluid will flow over it from above. However, one author, Connell, does not use this configuration. Instead, in his research, he pins the corners of the leading edge to more accurately replicate the behavior of a flag [4]. Regardless of the configuration used to dynamically model the flag, it is readily agreed upon that the deflection of the flag occurs in two directions [3,6]. Likewise, with this paper, the deflection of the flag is assumed to occur in two dimensions: along the length and width of the flag.

To successfully complete this paper, understanding the properties of the fluid is essential. Specifically, it is important to understand the interaction between the uniform flow and the flag, especially the differential pressure along the flag. For this paper, nonlinear vibrations and the associated pressure differential were studied under a constant flow [7-9]. Additionally, the majority of researchers agree that the fluid is inviscid [10]. Additionally, most researchers exploit the incompressible nature of the flow [11].

The tension in the flag caused by the uniform flow is the most disputed term when deriving the equation of motion. For instance, one author even models the tension differently in separate papers [2,5]. Essentially, one cannot find anyone in agreement on the best model of the tension within the flag. Some have linear tensions, some have differential tensions, while some have time averaged tensions [12-16].

The goal of this paper is to successfully model the dynamic vibrational response of a vertical flag under wind flow as a membrane. For this paper, the tension is caused by the weight of the flag. It is a constant tension given the orientation of the flag. Using the model, the mode shapes of the flag will be obtained when it is under a uniform fluid flow and a tension force due to gravity. Modeling the flag as a membrane and applying both Hamilton's principle and Galerkin's method, the equation of motion and the modal response will be able to be found. Then, the vibrations on different flag points, which will be defined in a moment, will be investigated and discussed.

DYNAMIC ANALYSIS

An energy approach is used to model the flag's system dynamics. In an attempt to more successfully capture the two-dimensional motion of the flag, it is modeled as a membrane with negligible stiffness. To begin modeling the flag, it is necessary to define the different energies in terms of the deflection at the surface. Fig. 1 portrays the system in question.

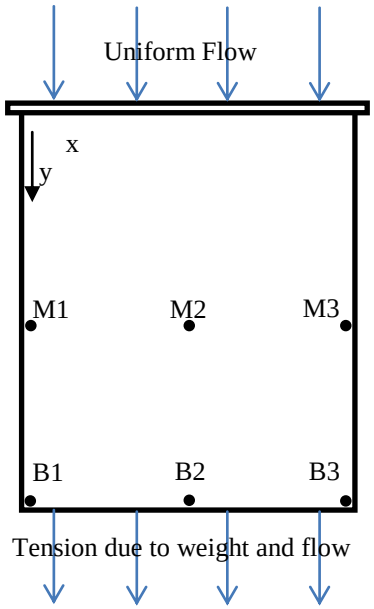

Fig. 1: Picture of the system being studied.

In Fig. 1, the individual points, M1, M2, M3, B1, B2, and B3, are the points that will be studied in the Results Section at different flow speeds. In this model, a constant tension is assumed in the vertical direction. Since the flag is oriented vertically, the constant tension is caused by the weight of the flag. The strain that the weight imposes affects the potential energy of the system.

$$V(t) = \int_A \vec{T} \cdot d\Delta \qquad (1)$$

By analyzing the geometry of a deformed section of the surface, the potential energy is written as

$$V(t) = \frac{1}{2}\iint_A T_y \left(\frac{\partial w}{\partial y}\right)^2 dA\,, \qquad (2)$$

where T_y is the scalar tension in the y-direction. This is equal to the product of the width, area density, and gravitational constant. Furthermore, the deflection of the surface, *w*, is a function of *x*, *y*, and *t*. The kinetic energy is defined as

$$KE(t) = \frac{1}{2}\int_A \rho \left(\frac{\partial w}{\partial t}\right)^2 dA\,, \qquad (3)$$

where ρ is the area density of the membrane. Knowing this, the Lagrangian of the system would be introduced as

$$L = \frac{1}{2}\iint_A \rho\left(\frac{\partial w}{\partial t}\right)^2 - T_y\left(\frac{\partial w}{\partial y}\right)^2 dA\,. \qquad (4)$$

If Hamilton's principle is then applied to the problem, the equation of motion and boundary conditions can be found. By allowing for virtual displacements, Eq. (4) becomes

$$\int_{t_1}^{t_2} (\delta L + \delta W^{nc}) dt = 0\,, \qquad (5)$$

where

$$\delta L = \iint_A \rho\left(\frac{\partial w}{\partial t}\right)\cdot\delta\left(\frac{\partial w}{\partial t}\right) - T_y\left(\frac{\partial w}{\partial y}\right) \cdot\delta\left(\frac{\partial w}{\partial y}\right) dA \qquad (6)$$

and

$$\delta W^{nc} = \iint_A p(x,y,t)\cdot\delta w\, dA\,. \qquad (7)$$

Eq. (7), the non-conservative work within the system, originates from the turbulence in the flow, which is caused by the interaction of the flag with the air flow. As one can see, Eq. (7) is expressed as a pressure term. When Eq. (6) is integrated by parts, the following is obtained

$$\int_{t_1}^{t_2}\left\{\iint_A T_y\left(\frac{\partial^2 w}{\partial y^2}\right) - \rho\left(\frac{\partial^2 w}{\partial t^2}\right) + p(x,y,t)\, dA\right\} dt + \oint_C T_y\left(\frac{\partial w}{\partial y}\right)\ell_x dC = 0\,, \qquad (8)$$

where *C* is the boundary of the flag and

$$\ell_x = \cos(x) \qquad (9)$$

where *x* is the angle between the two major axes of the flag. For this paper, the axes are perpendicular, so l_x is zero.

To satisfy the variational principle, the integrands of both terms in Eq. (8) must be zero. Thus, the equations of motion and boundary conditions for the flag are

$$T_y\frac{\partial^2 w}{\partial y^2} + p(x,y,t) = \rho\frac{\partial^2 w}{\partial t^2} \qquad (10)$$

$$w(x,0,t) = 0 \quad ; \quad T_y w_y(x,L,t) = 0$$
$$T_x w_x(0,y,t) = 0 \; ; \quad T_x w_x(h,y,t) = 0\,.$$

Since the effects of cross flow are considered to be negligible in this particular model, it is assumed that the tension in the x direction is zero.

Modal Analysis

Using the equation of motion, the mode shapes can be obtained via separation of variables. The deflection equation can be written as a product of three functions,

$$w(x,y,t) = \phi(x)\psi(y)q(t) \qquad (11)$$

which can now be substituted into the original partial differential equation. This is obtained by looking at the homogenous form of Eq. (10). The results of the spatial separation are then

$$\phi(x) = Asin(\alpha x) + Bcos(\alpha x)$$
$$\psi(y) = Csin(\gamma y) + Dcos(\gamma y), \qquad (12)$$

where

$$\alpha^2 + \gamma^2 = \beta^2 \qquad (13)$$

and

$$\beta = \omega\sqrt{\frac{\rho}{T_y}} = \frac{\omega}{c}\,. \qquad (14)$$

The natural frequencies are related to the mode shapes through the wave speed of the system, which can be seen in Eq. (13). Evaluating Eq. (11) and Eq. (13) yields the following combined mode shapes

$$W_{jk}(x,y) = C_{jk}sin\left(\frac{j\pi y}{2L}\right)\cos\left(\frac{k\pi x}{h}\right). \qquad (15)$$

Naturally, all mode shapes must satisfy the orthogonality condition. In result, the inner product between two identical modes must be one. Knowing this, the normalized mode shapes would be

$$W_{jk}(x,y) = \frac{2}{\sqrt{hL\rho^2}}sin\left(\frac{j\pi y}{2L}\right)\cos\left(\frac{k\pi x}{h}\right). \qquad (16)$$

and the natural frequencies

$$\omega_{jk} = \pi\sqrt{\frac{T_y}{\rho}}\left[\left(\frac{j}{2L}\right)^2 + \left(\frac{k}{h}\right)^2\right]^{1/2}. \qquad (17)$$

With the equation of motion and mode shapes solved for, it is necessary to find the forcing function, the pressure differential, acting on the system.

Pressure Differential

As stated before, deriving the pressure differential across the flag was studied extensively [7]. Needless to say, several assumptions need to be made to be able to model the pressure on the flag. These assumptions include assuming low air speed, sufficient flag width to assume minimal cross flow, and an approximation of the downstream motion of the flag. It is assumed that the air speed is low and the flag width sufficient based off previous wrok done [17].

First, the flow has some velocity potential, $\xi(x,y,z,t)$, that satisfies the following [7]

$$\nabla^2\xi - \frac{1}{a^2}\left(\frac{\partial}{\partial t} + V_{air}\frac{\partial}{\partial y}\right)^2 \xi = 0\,. \quad (18)$$

Eq. (17) is a form of Bernoulli's principle for incompressible flow, where a is the speed of sound in the fluid and V_{air} is the speed of the fluid. The formula for a velocity potential is

$$\mathbf{v} = \nabla\xi\,, \quad (19)$$

which can be substituted into Bernoulli's equation to determine an expression for the pressure variations on one side of the flag. Substituting Eq. (19) into Eq. (18), the pressure is written as

$$p_{\pm} = -\rho\left[\frac{\partial\xi}{\partial t} + V_{air}\frac{\partial\xi}{\partial y}\right]_{z=0}, \quad (20)$$

which is evaluated at the surface of the flag. Ultimately, to evaluate the solution to the potential equation, Eq. (18), a separable form must again be assumed, and the exact solution can be found with a summation of the resulting periodic separations.

For convenience and simplicity, the separated form of the velocity potential will be assumed from observation. This assumed potential is

$$\xi(x,y,z,t) = \hat{\xi}(x,z)\cdot\cos(\omega_{11}t - y), \quad (21)$$

where ω_{11} is the natural frequency of the first mode shape. The spatial function can then be separated into two spatial functions. These spatial functions will only be dependent on one variable each and can be solved by applying the boundary conditions at the vertical boundaries. Therefore, the complete solution is

$$\hat{\xi}(x,z) = \sum_{n=0}^{\infty} A_n e^{-q_n z}\cos\left(\frac{n\pi x}{h}\right) \quad (22)$$

where

$$q_n = \frac{\pi}{h}\left\{n^2 + \left(\frac{h\omega_{11}}{\pi c}\right)^2\left[1 - \left(\frac{V_{air}-c}{a}\right)^2\right]\right\}^{1/2}. \quad (23)$$

These coefficients, q_n, can be simplified by realizing that the difference between the air speed and the wave speed is significantly smaller than the speed of sound in the fluid. As a result, q_n may be simplified to

$$q_n = \frac{\pi}{h}\left\{n^2 + \left(\frac{h\omega_{11}}{\pi c}\right)^2\right\}^{1/2}. \quad (24)$$

Lastly, it is necessary to apply another approximation of the final solution for the deflection of the membrane to evaluate the coefficients of the potential modes, A_n. Therefore, in order to satisfy the surface condition, a solution of the following form is applied

$$\tilde{w}(x,y,t) = \hat{w}\sin\left(\frac{n\pi x}{h}\right)e^{i(\omega_{11}t - y)} \quad (25)$$

where $\hat{w}$ is a scaling factor that can be matched to empirical data. Applying this solution, the final pressure variation for one side of the flag turns out to be

$$p_{+} = -\frac{2\omega_{11}\rho(V_{air}-c)^2}{\pi c^2}\hat{w}\left[\frac{1}{q_0} - \sum_{n=1}^{\infty}\frac{2}{(4n^2-1)q_{2n}}\cos\left(\frac{2n\pi x}{h}\right)\right]\cos(w_{11}t - y) \quad (26)$$

Note, that this pressure variation is for one side of the flag. Exploiting the symmetry of the flag, this pressure variation can be doubled to find the pressure variation over the entire flag.

Now, Galerkin's method can be applied to solve for the response of the flag. Galerkin method minimizes the residual error generated from an assumed solution by forcing the inner product between the error and the comparison function to zero. The assumed solution will be the product of the mode shapes from the unforced problem and a set of time factors as in

$$\tilde{w}(x,y,t) = \sum_{j=1}^{J}\sum_{k=1}^{K} W_{jk}(x,y)\cdot Q_{jk}(t)\,. \quad (27)$$

Upon substituting this into the final equation of motion, the resulting partial differential equation is multiplied by each mode shape and then integrated with respect to the spatial boundaries. The result is a set of coupled ordinary differential equations in $Q_{jk}(T)$,

$$\mathbf{A}\{\ddot{Q}_{jk}\} + \mathbf{B}\{Q_{jk}\} = \mathbf{C}\cdot\cos(\omega_{11}t) + \mathbf{D}\cdot\sin(\omega_{11}t) + \mathbf{E}\,, \quad (28)$$

where A, B, C, D, and E are matrices of constant coefficients. Once the set can be written into state space, the time factors and their derivatives are expressed as a set of generalized coordinates where

$$\{\dot{G}_{jk}\} = -\mathbf{B}\cdot\mathbf{A}^{-1}\{G_{jk}\} + \mathbf{C}\cdot\mathbf{A}^{-1}\cos(\omega_{11}t) + \mathbf{D}\cdot\mathbf{A}^{-1}\sin(\omega_{11}t) + \mathbf{E}\cdot\mathbf{A}^{-1}\,. \quad (29)$$

This will then be numerically solved in the Results Section. Doing so will give a representation of the response of the flag.

RESULTS

The results obtained through numerical simulations are consistent with observational data [17]. For the numerical analysis, the air speed was set to be 5 m/s since it represents a regular wind speed and the scalar factor is equal to one. Tab. 1, tabulates the values used to find the mode shapes of the flag. Figures 2 to 5 show the first four mode shapes. Please note that the z-axis in Figures 2-5 capture the modal response, not the deflection of the system.

Property	Value
Young's Modulus	3 GPa
Shear Modulus	3 GPa
Poisson's Ratio	0.5
Density	0.137 kg/m^3
Length	0.152 m
Width	0.076 m
Thickness	0.00013 m

Tab. 1: Physical and geometrical properties of the flag.

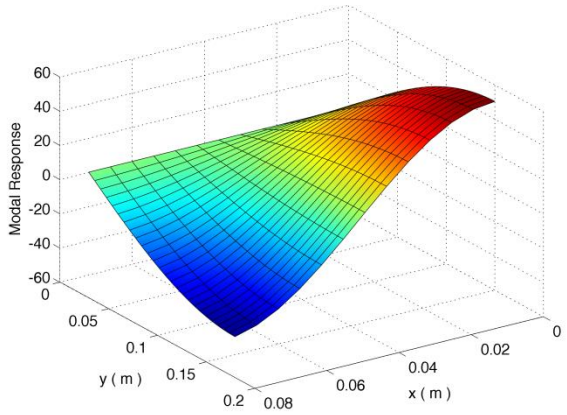

Fig. 2: Mode (1,1) of the Flag.

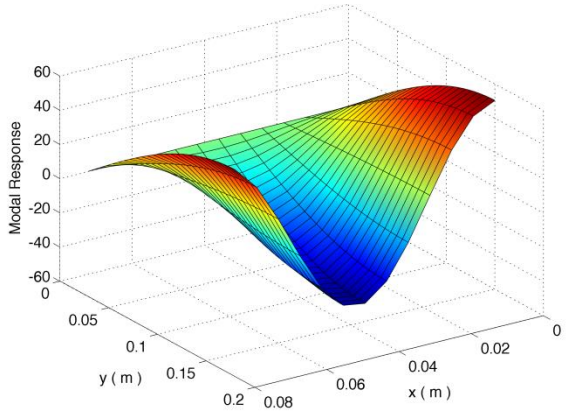

Fig. 3: Mode (1,2) of the Flag.

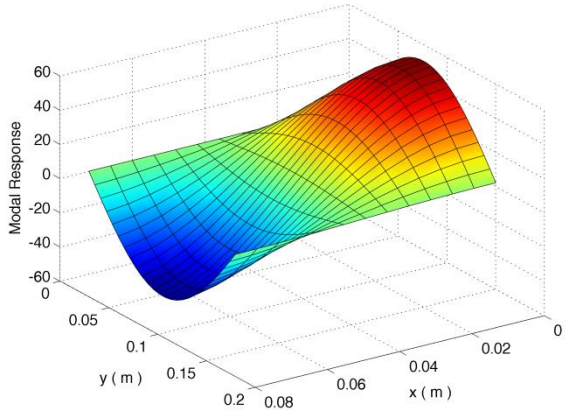

Fig. 4: Mode (2,1) of the Flag.

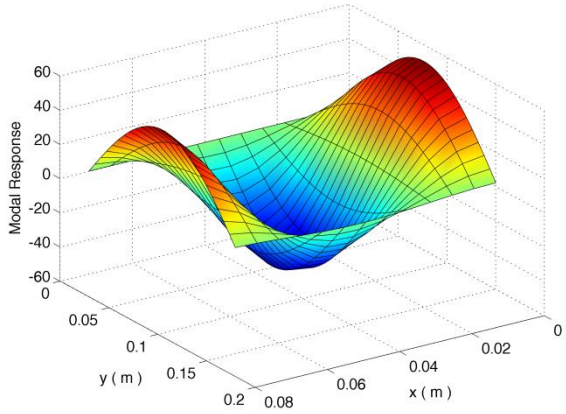

Fig. 5: Mode (2,2) of the Flag.

The amplitudes of the above figures are not representative of the response of the system. However, they do in fact indicate each mode's contribution to the final response.

Fig. 6 shows the response of the flag to the input pressure of wind flow. In the numerical analysis, all first four modes have been considered. It is in this figure that one can see the contribution of each of the above modes to the final response.

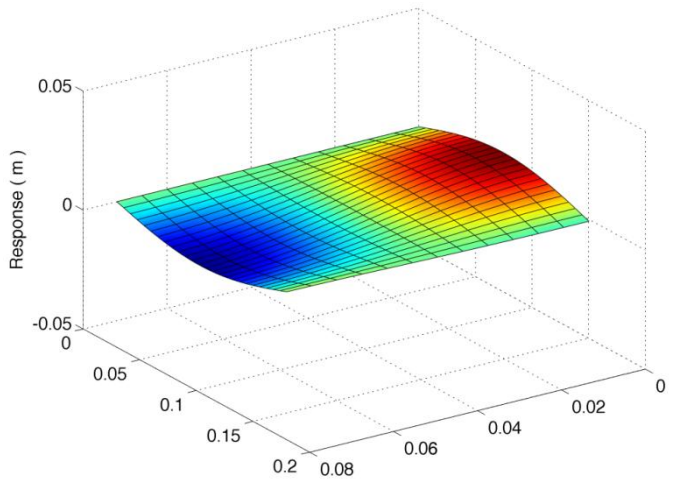

Fig. 6: Response of the flag halfway through an oscillation cycle

The time evolution shows considerable deflection in the flow direction but minimal deflection on the free end. This correlates with the assumptions made to find this solution. To further study the results, the deflection through time at given points along the flag has been investigated. To understand the location of the points on the flag, it will be useful to refer to Fig. 1. Furthermore, Tab. 2 defines the exact location of the points labeled in Fig. 1.

Point	Location	Line Type	Line Color
M1	(0.0076, 0.076)	Solid	Black
M2	(0.038, 0.076)	Dashed	Red
M3	(0.0684, .076)	Dashed with x's	Blue
B1	(0.0076, 0.152)	Solid	Black
B2	(0.038, 0.152)	Dashed	Red
B3	(0.0684, 0.152)	Dashed with x's	Blue

Tab. 2: Exact location and line descriptions for flag's investigated points.

In referring to both Fig. 1 and Tab. 2, this paper investigated the deflection at the six points mentioned above. M1, M2, and M3 correspond to the three points along the center of the flag. Similarly, B1, B2, and B3 refer to the three points along the end of the flag. Tab. 2 also defines the line type for each point on the flag. Lastly, the fluid velocities studied in the following analysis are 5 m/s, 7 m/s, 9 m/s, and 11 m/s. These velocities were chosen based off of the experimental investigations in the wind tunnel. Ultimately, one can see the effect of the wind speed when one observes the flag in the wind tunnel. At low wind speeds, the vibrations of the flag are not complete, whereas at high wind speeds the deflection of the flag occurs with slow, quick amplitudes. In other words, the amplitude is small, for it is vibrating very quickly. Previous work has determined that the most desirable range of velocity is 15-25 mph. By choosing 5 m/s, 7 m/s, 9 m/s, and 11 m/s, a range of 11.2-24.6 mph is covered [17-18].

Here, the deflections in center point will be studied first. These points are M1, M2 and M3. Fig. 7 shows the deflection at the center of the flag when the fluid velocity is 5 m/s.

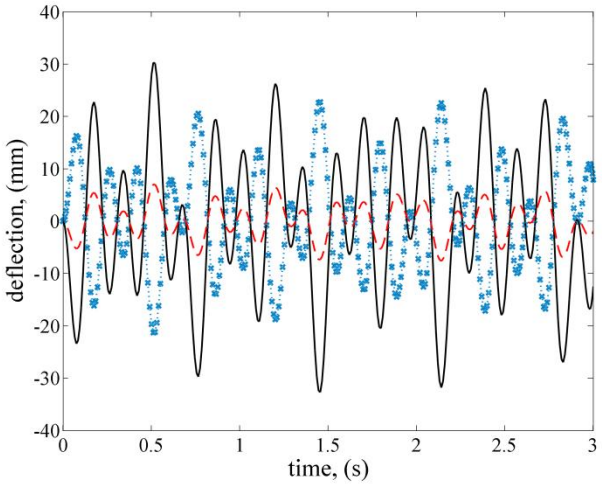

Fig. 7: Deflection of the three points in the middle of the flag when velocity is 5 m/s

From Fig. 7, it is apparent that the points on the edges of the flag experiences considerably more deflection than the middle of the flag. This is further confirmed by observing the deflection at the end of the flag. Figure 8 shows the vibration deflections for points B1, B2, and B3 at the free -end of the flag.

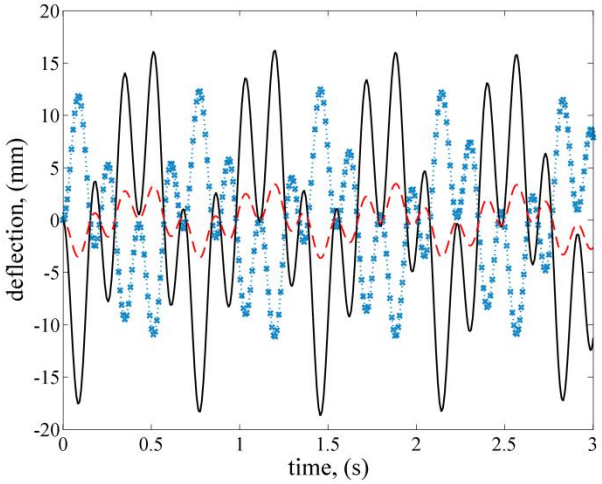

Fig. 8: Deflection of the three points at the free-end when velocity is 5 m/s

Fig. 8 confirms what is observed in Fig. 7. However, one can see that the amplitudes on the edges in Fig. 7 are slightly larger than those found in Fig. 8, yet the amplitudes at the middle of

the flag seem to be slightly larger at the end of the flag. Likewise, it seems that the amplitude at the bottom of the flag is the greatest. This is due to considering four modes together.

To further explore this, graphs were constructed when the velocity was assigned a value of 11 m/s. Fig. 9 shows the deflections of points B1, B2, and B3 at the center of the flag when the velocity is 11 m/s.

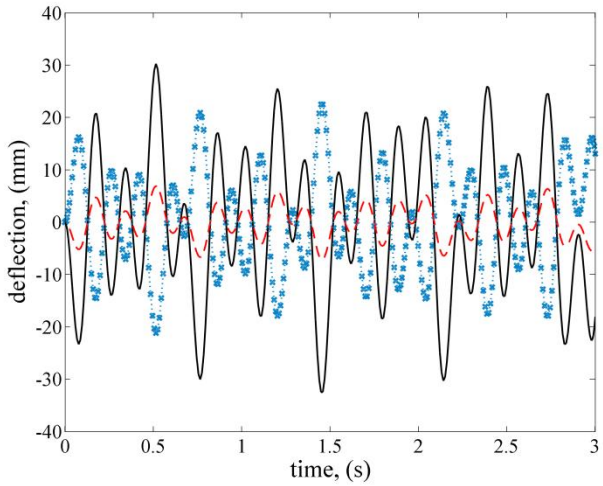

Fig. 9: Deflection of the three points in the middle of the flag when velocity is 11 m/s

Similar to when the velocity was 5 m/s, the same trends are apparent. Likewise, the added velocity did not greatly affect the deflection. This is further seen by the deflections portrayed in Fig. 10 for points M1, M2, and M3 at the free-end of the flag.

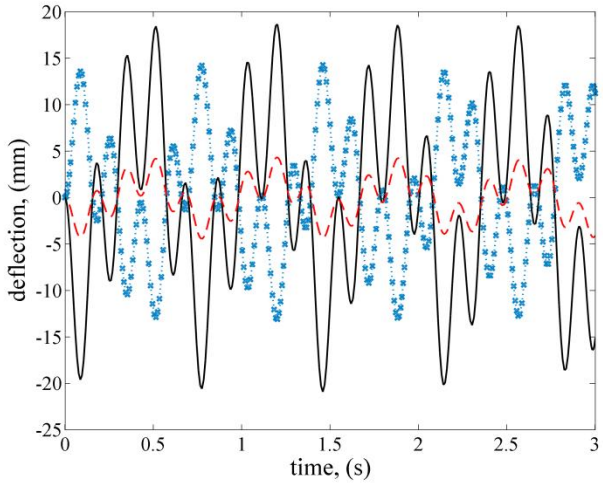

Fig. 10: Deflection of the three points at the free-end when velocity is 11 m/s

Yet again, the same trends are present in this graph. It seems to show that the velocity, at least within the presented model, does not have a large effect. It would be interesting to see what amplitudes would be expected if the velocity were dramatically increased.

While the above graphs do not show a terribly large change of deflection as the velocity increases, it is readily apparent when one glances at the root mean square deflection at each point at different velocities. Adjusting the velocity from 5 m/s to 11 m/s in increments of two, graphing the deflection, then finding the root mean square deflection yields Tab. 3.

Point	5 m/s	7 m/s	9 m/s	11 m/s
M1	13.938	13.695	13.711	13.841
M2	3.288	3.105	3.691	3.150
M3	9.823	9.556	9.775	9.662
B1	8.771	9.644	9.968	9.991
B2	1.780	2.079	3.520	2.210
B3	5.917	6.632	7.306	6.892

Tab. 3: Root Mean Square deflections of each point at different velocities.

Tab. 3 shows the root mean square (RMS) deflection at each of the described points at different velocities. The RMS analysis was chosen because it is believed it would accurately capture the deflections of the system. Before choosing this method, the highest and lowest deflection in each scenario was averaged to obtain an average deflection. Understandably, this seemed insufficient [17]. Note that generally the RMS deflection increases as the velocity increases. However, at some points, especially M2 and B2, the RMS decreases at 11 m/s. The cause of this may be due to the accumulation of the mode shapes. Another possible reason for this variation is the exclusion of nonlinearities in the system. While nonlinearities are certainly present, this paper does not take these into account.

CONCLUSION

A flag was modeled to study the deflection of the flag in response to wind flow and tension due to gravity. Applying Hamilton's principle and the Galerkin method, the partial differential equation of motion and the first four mode shapes were found. The pressure differential along the flag was found by studying the flags interaction with the velocity field. Once the partial differential equation of motion and the first mode shapes were found, the flag response was studied by changing the velocity of the flow. As the velocity increases the deflection of the flag also increases. More importantly, there seemed to be a significant jump in the deflection between 9 m/s and 11 m/s. This seems to imply that a critical speed was reached within the system.

REFERENCES

[1] Howell, R. M., Lucey, A. D., Carpenter, P. W., 2009, "Interaction between a Cantilevered-Free Flexible Plate and Ideal Flow," Journal of Fluids and Structures, 25(3) pp. 544-566.

[2] Moretti, P. M., 2004, "Flag Flutter Amplitudes," Flow Induced Vibrations, Anonymous de Langre & Axisa ed., Ecole Polytechnique, Paris, I, pp. 113-118.

[3] Doaré, O., and Michelin, S., 2011, "Piezoelectric Coupling in Energy-Harvesting Fluttering Flexible Plates: Linear Stability Analysis and Conversion Efficiency," Journal of Fluids and Structures, 27(8) pp. 1357-1375.

[4] Connell, B. S. H., and Yue, D. K. P., 2007, "Flapping Dynamics of a Flag in a Uniform Stream," Journal of Fluid Mechanics, 581pp. 33-67.

[5] Moretti, P. M., 2002, "Flutter in Webs," Flutter in Webs, Anonymous T.U. Darmstadt, Kaiserslautern, Germany.

[6] Martin, A., 2006, "Experimental Study of Drag from a Fluttering Flag." Master's Thesis. Oklahoma State University, Stillwater.

[7] Chang, Y.B., Moretti, P.M., 2002, "Flow Induced Vibration of Free Edges of Thin Films," Journal of Fluids and Structures, 16(7) pp. 989-1008.

[8] Watanabe, Y., Isogai, K., Suzuki, S., 2002, "A Theoretical Study of Paper Flutter," Journal of Fluids and Structures, 16(4) pp. 543-560.

[9] Watanabe, Y., Suzuki, S., Sugihara, M., Sueoka, Y., 2001, "An Experimental Study of Paper Flutter," Journal of Fluids and Structures, 16(4) pp. 529-542.

[10] Alben, S., Shelley, M., 2008, "Flapping States of a Flag in an Inviscid Fluid: Bistability and the Transition to Chaos," Physical Review Letters, 074301 pp. 1-4.

[11] Michelin, S., Smith, S. G. L., and Glover, B. J., 2008, "Vortex Shedding Model of a Flapping Flag," Journal of Fluid Mechanics, 617pp. 1-10.

[12] Argentina, M., Mahadevan, L., 2004, "Fluid-Flow-Induced Flutter of a Flag," Proceedings of the National Academy of Sciences, 102(6) pp. 1829-1834.

[13] Manela, A., Howe, M.S., 2009, "The Forced Motion of a Flag," Journal of Fluid Mechanics, 635 pp. 439-454.

[14] Tang, L., Paidoussis, M., 2007, "On the Instability and the Post-Critical Behaviour of Two-Dimensional Cantilevered Flexible Plates in Axial Flow," Journal of Sound and Vibration, 305 pp. 97-115.

[15] Semler, C., Li, G. X., Paidoussis, M.P., 1992, "The Non-Linear Equations of Motion of Pipes Conveying Fluid," Journal of Sound and Vibration, 169(5) pp. 577-599.

[16] Moretti, P., 2003, "Tension in Fluttering Flags," Proceedings of the Tenth International Congress on Sound and Vibration, pp. 1-8.

[17] Truitt, A., Mahmoodi, S. N., 2013, "A Review on Active Wind Energy Harvesting Designs," International Journal of Precision Engineering and Manufacturing, 14(9) pp. 1667-1675.

[18] Wynn, L., Truitt, A., Heim, I., Mahmoodi, S. N., 2013, "Modeling and Response Analysis of Piezoelectric Flag in Wind Flow," Proceedings of the Dynamic Systems and Control Conference, pp. 1-8.